ACS APPLIED MATERIALS & INTERFACES

Research Article

www.acsami.org

Lithium Compound Deposition on Mesocarbon Microbead Anode of Lithium Ion Batteries after Long-Term Cycling

Lijie Yang, Xinqun Cheng,* Yunzhi Gao, Pengjian Zuo, Yulin Ma, Chunyu Du, Bin Shen, Yingzhi Cui, Ting Guan, and Geping Yin*

Institute of Advanced Chemical Power Sources, School of Chemical Engineering and Technology, Harbin Institute of Technology, Harbin 150001, China

ABSTRACT: Lithium compound deposition on mesocarbon microbead (MCMB) anode after long-term cycling was studied in $LiCoO_2$/MCMB battery. Lithium compound deposition did not generate on the activated MCMB anode, but it generated unevenly on the long-term cycled anode. Gray deposition composed of dendrites and particles was formed on the lower surface of the MCMB layer first, then on the upper surface. The deposition and MCMB layer peeled off from the current collector, and a bump was formed in the cycled anode. The exfoliation and thick deposition increased the ohmic resistance, film resistance, and charge transfer resistance of the cell and decreased the capacity significantly. Metallic lithium did not exist in either the upper or the lower deposition layer according to the results of X-ray photoelectron spectroscopy (XPS), X-ray diffraction (XRD), the discharge curve, and anode potential. The outer region of both the lower and the upper deposition layers consisted of Li_2CO_3, LiOH, $ROCO_2Li$, and ROLi. The inner region of the etched lower deposition layer mainly consisted of Li_2O, LiF, and Li_2CO_3, and that of the etched upper deposition layer mainly consisted of Li_2CO_3, $ROCO_2Li$, ROLi, and LiF. Solid electrolyte interphase (SEI) film hindering the intercalation of lithium ions into carbon layers and $LiCoO_2$ cathode providing lithium source for the deposition were the two reasons leading to the formation of lithium compound deposition during long-term cycles. Because SEI film on the lower surface of MCMB layer was thicker than that on the upper surface, lithium compound deposition generated on the lower surface first.

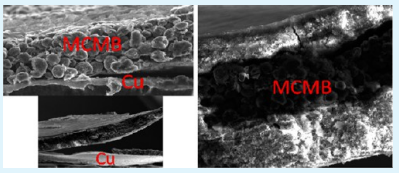

KEYWORDS: *lithium ion batteries, lithium compound deposition, mesocarbon microbead, long-term cycling, solid electrolyte interphase film*

1. INTRODUCTION

Metallic lithium has been applied widely in early lithium battery and novel battery systems, such as Li/air[1,2] and Li/sulfur batteries.[3,4] Dendritic lithium deposition could be observed in these metallic lithium anodes.[5−10] The deposition could lead to an internal short circuit and made the battery dangerous.

Because the working potential of graphite anode was very close to that of metallic lithium,[11] lithium deposition might also appear on graphite anode in some situations and affected the safety and life of the lithium ion battery. When the capacity ratio of anode to cathode (A/C) was too low, metallic lithium might be deposited on graphite anode.[12] Besides the unreasonable design of the battery, special service conditions could also lead to the formation of lithium deposition, such as overcharging,[13,14] charging at large current, or low temperature.[15] Because graphite layer was fully lithium intercalated and anode potential decreased below 0 V during the overcharging, excessive lithium ions from the cathode would generate tubular-like metallic lithium deposition on graphite anode. Lithium deposition reacted with electrolyte to form a solid electrolyte interphase (SEI) film, and the behavior was similar to that of metallic lithium anode in lithium battery.[16] When the full battery was charged at large current or low temperature, anode potential could also decrease below 0 V, leading to the generation of lithium metal.[17] The anode polarization under such conditions was greater than cathode polarization, so anode dominated the performance decline of full battery.[15,18−21]

In our study, gray depositions with the morphology similar to lithium deposition could be observed on mesocarbon microbead (MCMB) anode after long-term charge/discharge cycling, and these depositions were identified as lithium compounds by X-ray photoelectron spectroscopy (XPS). However, less work was devoted to the study of lithium compound deposition during long-term cycling. In this experiment, the morphology, effects on the performance of battery, composition, and formation mechanism of lithium compound deposition were evaluated in $LiCoO_2$/MCMB battery.

2. EXPERIMENTAL SECTION

$LiCoO_2$/MCMB battery used in this experiment had a nominal capacity of 1150 mAh. The cathode was prepared by coating $LiCoO_2$ (910H, produced by Pulead Co. of China), acetylene black (AB), and polyvinylidene fluoride (PVDF) on aluminum (Al) foil, and the anode was prepared by coating MCMB (CMS-G15, produced by Shanshan Co. of China), AB, and PVDF on copper (Cu) foil. The electrolyte was 1 mol/L $LiPF_6$ dissolved in ethylene carbonate/diethyl carbonate/ethyl methyl carbonate (EC/DEC/EMC, 1:1:1 by volume).

Received: May 10, 2014
Accepted: July 14, 2014
Published: July 14, 2014

The battery was charged with the constant-current/constant-voltage method (0.6 C, 4.2 V, until the current was below 0.02 C). After a rest of 2 min, the battery was discharged at 0.6 C, and the discharged capacity was 30% of nominal capacity. The battery was charged and discharged for 3200 cycles, and capacity verification was conducted at 0.2 C within the voltage range of 2.75−4.2 V before and after the cycling at 0.6 C. The battery without the cycling and with capacity verification was abbreviated as activated battery.

Batteries after activation and long-term cycles were dismantled in the Ar-filled glovebox. The obtained plate group including cathode, anode, and separator was put into fresh electrolyte, along with the reference electrode (RE) of metal lithium plate. Anode potential (vs Li^+/Li) was monitored when the full battery was charged and discharged at 1 C within the range of 2.75−4.2 V. Morphology of the obtained cycled MCMB anode was recorded by digital camera. The activated and cycled anodes then were soaked in dimethyl carbonate (DMC) to remove the electrolyte salt $LiPF_6$, and cross-sectional morphologies were characterized by scanning electron microscopy (SEM, Helios Nanolab 600i). XPS depth analysis (K-Alpha, Thermofisher Scientific) was performed by etching of Ar-ion on the cycled anode.

To examine the effect of lithium compound deposition on the anode performance, MCMB material was removed by *N*-methyl-2-pyrrolidone (NMP) from one side of the cycled anode. Anode disks (the diameter of 14 mm, Φ) with or without lithium compound deposition then were punched from the different regions of cycled anode in glovebox. The coin cell (model 2025) was assembled using MCMB electrode disk and lithium foil. Electrochemical impedance spectroscopy (EIS) was conducted at the lithiated state with the frequency range of 0.01−100 000 Hz and the amplitude of 5 mV. Coin cell was charged and discharged at 0.02 C within the voltage range of 0.01−1.5 V (vs Li^+/Li).

The Φ14 mm cycled anode disk without lithium compound deposition was further soaked in H_2O to remove SEI film on the surface of cycled anode. In addition, pristine anode disk was also prepared by punching from pristine MCMB anode. These disks were assembled into coin cells and charged/discharged under the same conditions as described above.

To study the growth of SEI film during the long-term cycling and the effectiveness of water washing SEI film, surface morphologies of anodes after different cycles and water-washed anode were examined by SEM.

Anode samples obtained from activated and cycled batteries at fully charged state were sealed with polyethylene (PE) and tested by X-ray diffraction (XRD, PANalytical X'Pert PRO). Pristine cathode (PC) and cycled cathode regions corresponding to cycled anode regions without and with lithium compound deposition (abbreviated as NC and LC, respectively) from the cycled battery at fully discharged state were examined by XRD tests.

3. RESULTS AND DISCUSSION

3.1. Morphology of Deposition on Cycled MCMB Anode. According to the charge/discharge curves in Figure 1, the capacity of pristine $LiCoO_2$/MCMB battery at 0.2 C was 1183.9 mAh. After 3200 cycles, the capacity decreased to 973.1 mAh, and the capacity retention was 82.2%.

Figure 2 showed MCMB anode from the $LiCoO_2$/MCMB battery after 3200 cycles. A gray substance appeared on MCMB anode, and the distribution was nonuniform. In addition, a bump appeared on the position having the gray substance. Anode sample was obtained from the region with bump. The upper and lower surfaces of the sample then were examined by a digital camera and SEM (Figure 3). Gray substances appeared on both the upper and the lower surfaces of the anode sample (Figure 3a and c), and the substances on the two surfaces were both composed of dendrites and particles (Figure 3b and d). Such morphology was similar to that of lithium deposition.[6,8,13] It could be seen that gray deposition appeared unevenly on the upper surface of anode sample, and the region without deposition showed black (Figure 3a). Yet the gray deposition spread over almost the whole lower surface except for the edge

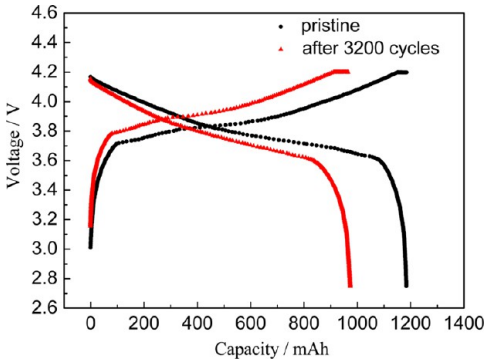

Figure 1. Charge/discharge curves of pristine $LiCoO_2$/MCMB battery and the battery after 3200 cycles (0.2 C).

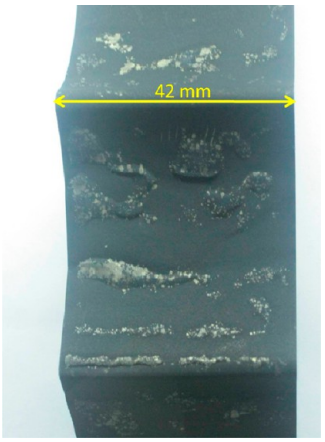

Figure 2. MCMB anode of the $LiCoO_2$/MCMB battery after 3200 cycles.

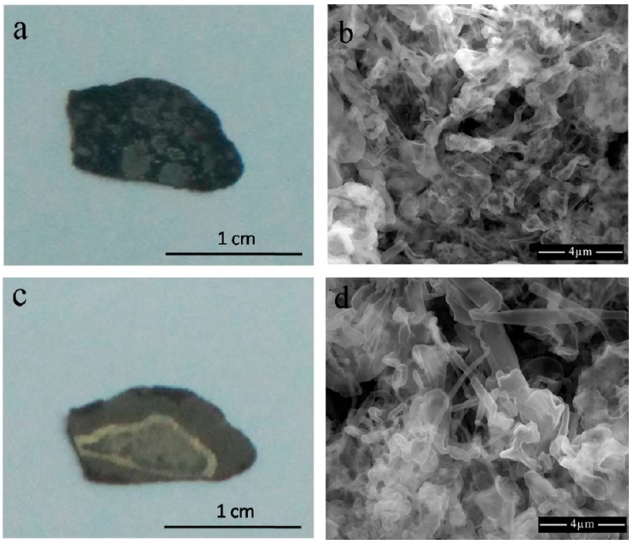

Figure 3. Digital photographs and SEM images of gray substance on the upper and lower surfaces of MCMB anode. (a) Digital photograph of the upper surface of MCMB anode, (b) SEM image of gray substance on the upper surface of MCMB anode, (c) digital photograph of the lower surface of MCMB anode, and (d) SEM image of gray substance on the lower surface of MCMB anode.

dx.doi.org/10.1021/am502887v | *ACS Appl. Mater. Interfaces* 2014, 6, 12962−12970

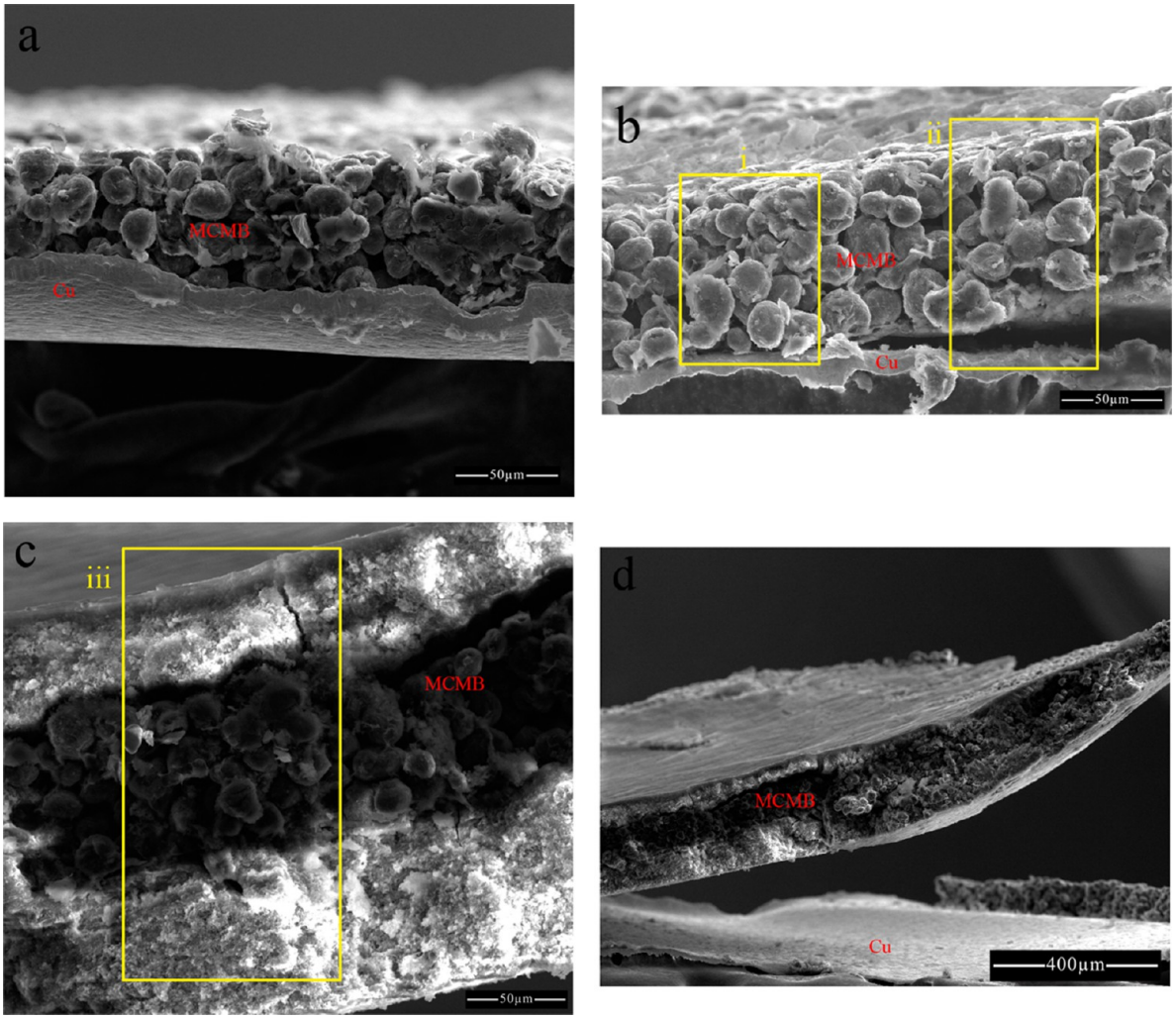

Figure 4. Cross-sectional SEM images of activated and cycled anodes. (a) Activated anode, (b–d) cycled anode.

of sample (Figure 3c). In other words, when the deposition did not appear in some regions of the upper surface of MCMB material, it has already appeared in the corresponding regions of the lower surface of MCMB material.

Figure 4 shows cross-sectional SEM images of activated and cycled anodes. It could be seen from Figure 4a that the thickness of Cu foil and MCMB material layer was 5 and 50 μm, respectively. Deposition was not found in the activated anode. Three different regions appeared in the cycled anode according to Figure 4b–d. MCMB particles were in direct contact with the current collector in region i. The deposition generated below MCMB layer in region ii, but it did not generate above MCMB layer. Deposition appeared both above and below MCMB layer in region iii, and the thickness of lower deposition (about 100 μm, Figure 4c) was larger than that of upper deposition (about 60 μm, Figure 4c) significantly. Therefore, it could be speculated that the deposition generated on the lower surface of MCMB layer first, and then on the upper surface of MCMB layer according to cross-sectional SEM images in Figure 4 and digital photographs in Figure 3. In addition, it could be seen that once the deposition appeared below MCMB layer, deposition layer and MCMB layer would peel off from Cu foil, which caused a bump to occur on the anode.

3.2. Effects of Deposition on the Electrochemical Properties of MCMB Anode Examined by EIS and Constant-Current Charge/Discharge Tests. EIS curves of cycled anodes with and without deposition were compared in Figure 5, and the equivalent circuit parameters obtained from the fitting are listed in Table 1. The adopted equivalent circuit has already been elaborated in our previous study.[11] Ohmic resistance of anode with deposition was larger than that without deposition due to the exfoliation between MCMB layer and

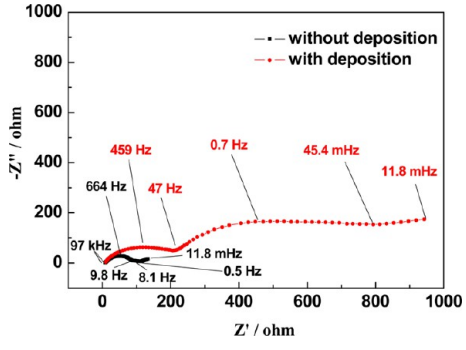

Figure 5. EIS curves of cycled MCMB anodes with and without deposition.

dx.doi.org/10.1021/am502887v | ACS Appl. Mater. Interfaces 2014, 6, 12962–12970

Table 1. Equivalent Circuit Parameters Obtained from EIS Curves of Cycled MCMB Anodes with and without Deposition

equivalent circuit parameters	without deposition	with deposition
ohmic resistance (Ω)	6.4	7.5
film resistance (Ω)	68.1	175.9
film capacitance (μF)	20.0	13.5
charge transfer resistance (Ω)	61.3	713.0
double-layer capacitance (mF)	9.0	0.7

current collector. Because the deposition formed on the upper and lower surfaces of MCMB material was very thick, which ranged from dozens of micrometers to nearly 100 μm, film resistance of anode with deposition was obviously larger. The surfaces of many MCMB particles were covered by thick deposition, leading to the decrease of active mass surface. Charge transfer resistance was inversely proportional to active mass surface, and double-layer capacitance was proportional to active mass surface.[22,23] Accordingly, charge transfer resistance and double-layer capacitance of anode with deposition increased and decreased significantly, respectively.

Figure 6 showed charge/discharge curves of cycled MCMB anodes with and without deposition. Delithiated capacity of

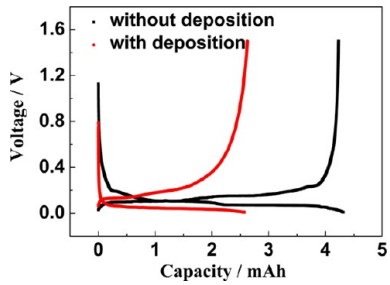

Figure 6. Charge/discharge curves of cycled MCMB anodes with and without deposition.

MCMB anode with deposition was 2.62 mAh, and that without deposition was 4.23 mAh. So capacity was reduced by 38.0% after the emergence of deposition. Moreover, platform voltage differences between charge and discharge increased after the deposition appeared on the anode. These declines of performances were related to the exfoliation of MCMB layer from Cu foil and the formation of thick deposition.

3.3. Compositions of Depositions and the Decline of Lithium-Intercalation Amount in Cycled Anode. Compositions of the depositions on the upper and lower surfaces of MCMB layer were examined by XPS with Ar-ion etching, and the results are shown in Figure 7. For the lower deposition layer, metallic lithium did not appear during Ar-ion etching for 180 min according to Li 1s spectra in Figure 7a. Because the etching rate was 0.3 nm/s, the etching depth of 180 min was 3.24 μm. Therefore, there was no metallic lithium in deposition layer within the depth of 3.24 μm. Obvious peaks of Li_2CO_3, LiOH, and $ROCO_2Li$ all existed when the sample was etched for 0−180 min. CO_3^{2-} could be observed in the whole etched deposition layer according to C 1s and O 1s spectra. The intensity of C−C peak (coming from $ROCO_2Li$ and ROLi) tended to decrease with the etching, indicating that the content of C−C in the outer region of etched layer was larger than that in the inner region. Because Li, C, and O were the main elements in the outer region of the lower deposition layer according to the depth profiles in Figure 7e, the outer region of the lower deposition layer mainly consisted of Li_2CO_3, LiOH, $ROCO_2Li$, and ROLi.

The peak of Li_2O did not appear during the etching of the first 10 s in Li 1s and O 1s spectra. Yet the peak could be observed after Ar-ion etching for 20 min, and its intensity increased with the etching, indicating that Li_2O existed in the interior of the etched deposition layer. Very weak peaks of LiF and P−F could be observed in Li 1s and F 1s spectra before etching and after etching for 10 s. The peak intensity of LiF increased apparently after etching for 20 min and then remained nearly constant during the following etching. So LiF mainly existed in the inner region of the etched deposition layer. Because an obvious CO_3^{2-} peak existed during the whole etching process and the peak intensity of C−C decreased with the etching, more Li_2CO_3 and fewer $ROCO_2Li$ were contained in the inner region. Accordingly, the inner region of the etched lower deposition layer mainly consisted of Li_2O, LiF, and Li_2CO_3.

For the upper deposition layer, metallic lithium did not exist during the whole etching process according to Li 1s spectra in Figure 7f. Obvious peaks of Li_2CO_3, LiOH, and $ROCO_2Li$ appeared during the etching of the first 20 min (within the thickness of 0.36 μm). Yet the peak intensity decreased significantly during the etching from 40 to 180 min (the thickness ranged from 0.72 to 3.24 μm). With the etching, the intensity of the C−C peak decreased significantly, and the intensity of the CO_3^{2-} peak decreased slightly in C 1s spectra. Because the relative content of C decreased with the etching in the depth profiles in Figure 7j, the outer region of the upper deposition layer mainly consisted of Li_2CO_3, LiOH, $ROCO_2Li$, and ROLi.

The obvious peak of CO_3^{2-} appeared during the whole etching according to C 1s and O 1s spectra, so CO_3^{2-} also existed in the inner region of the etched deposition layer. Although the intensity of C−C was decreased with the etching according to Figure 7g, it was still large in the later stage of the etching. So C−C also existed in the inner region of etched deposition layer. The intensity of LiF peak in Li 1s curves increased slightly during the etching of the first 20 min, and the peak was very obvious during the etching from 40 to 180 min. Weak peaks of LiF and P−F appeared in the F 1s curves before the etching and after the etching of 10 s. The intensity of LiF peak increased greatly from the etching of 20 min, and it remained almost constant during the following etching. Accordingly, LiF mainly existed in the inner region of the etched layer. Li_2O did not appear during the etching of first 20 min according to O 1s spectra in Figure 7h. It began to appear from the etching of 40 min, and the peak intensity increased slightly with the etching. In addition, the peak of Li_2O hardly appeared in Li 1s spectra (Figure 7f) in the whole etching. So the content of Li_2O was very low in the entire etched deposition layer. Accordingly, the inner region of the etched upper deposition layer was mainly composed of Li_2CO_3, $ROCO_2Li$, ROLi, and LiF based on the above results.

In summary, metallic lithium was not observed in either the upper or the lower deposition layer within the etching thickness of 3.24 μm. Moreover, the outer region of the two deposition layers consisted of Li_2CO_3, LiOH, $ROCO_2Li$, and ROLi. However, the inner region of etched upper and lower deposition layers had different compositions. The inner region of the etched lower deposition layer mainly consisted of Li_2O,

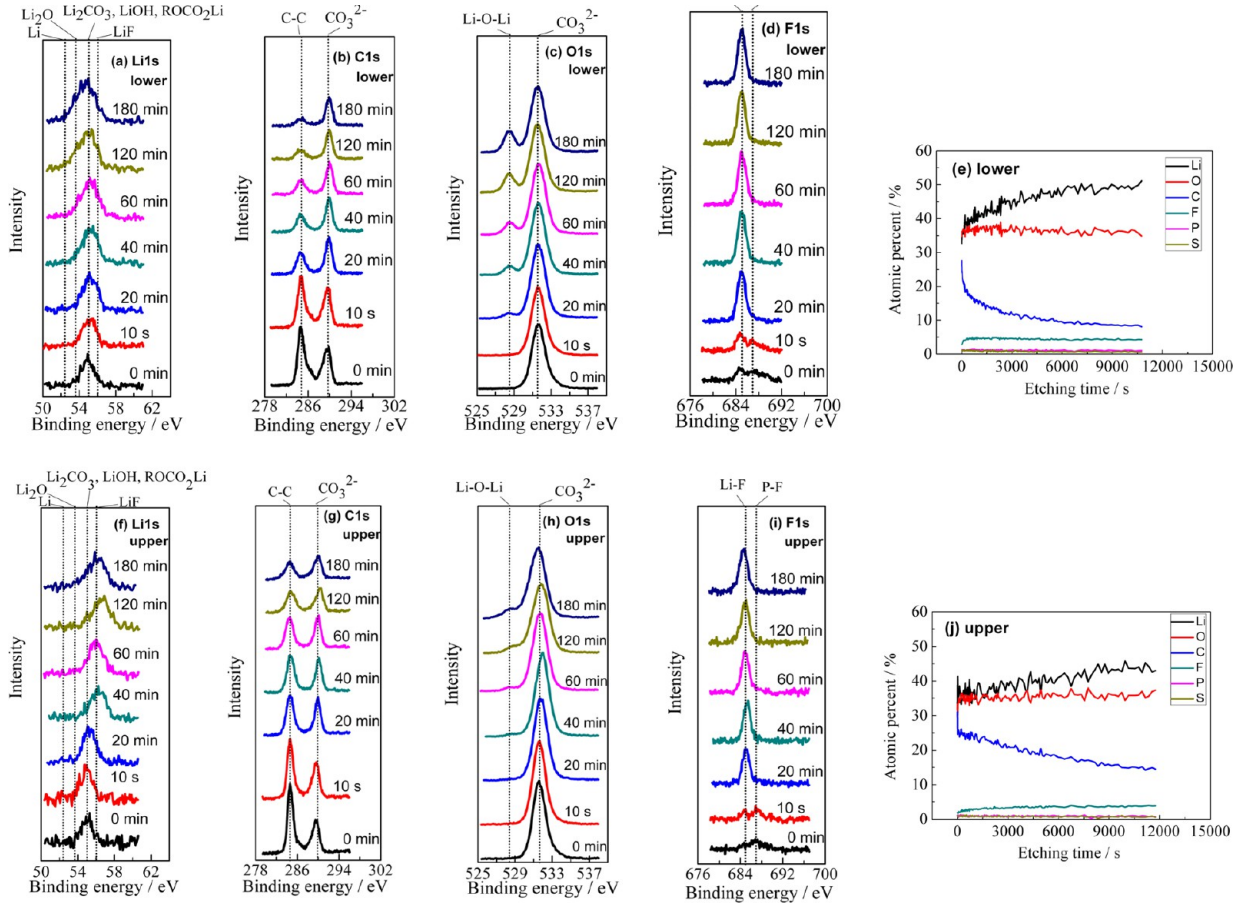

Figure 7. XPS spectra of Li 1s, C 1s, O 1s, and F 1s and depth profiles of depositions on the lower and upper surfaces of MCMB anode. (a–e) Depositions on the lower surface of MCMB, (f–j) depositions on the upper surface of MCMB.

LiF, and Li_2CO_3, and that of the etched upper deposition layer mainly consisted of Li_2CO_3, $ROCO_2Li$, ROLi, and LiF.

Obvious peaks of LiC_6 and LiC_{12} appeared in the XRD pattern (Figure 8) of activated anode. The intensity of LiC_6

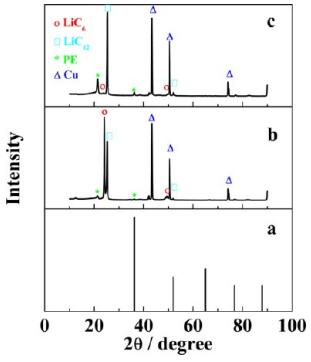

Figure 8. XRD patterns of Li, activated anode, and cycled anode with deposition. (a) Standard XRD pattern of Li, (b) activated anode, and (c) cycled anode with deposition.

(24.0°) was stronger than that of LiC_{12} (25.2°). The peak intensity of LiC_6 in the XRD pattern of cycled anode with deposition was very weak, and the intensity of LiC_{12} was much stronger than that of LiC_6 significantly. The results indicated that although the full batteries after the activation and long-term cycles were both fully charged, the amount of intercalated lithium in cycled anode with deposition was obviously less than that in activated anode. Accordingly, it could be speculated that lithium ions had more difficulty entering the carbon layer of cycled anode as compared to activated anode. Therefore, lithium ions gathered on the surface of MCMB particles to form the deposition.

The peak of metallic lithium at 36.2° overlapped with the peak of PE, and that at 52.0° overlapped with the peak of LiC_{12}. However, the peaks of metallic lithium at other positions (64.9°, 76.6°, and 87.9°) did not appear. Accordingly, metallic lithium was not detected in the deposition by XRD.

Figure 9 showed the voltage–time curves of activated and cycled full batteries charged and discharged at 1 C and the corresponding potential of MCMB anodes. When the full battery was charged and discharged, the anode potential of activated battery was in the range of 0.01–0.35 V, and that of cycled battery was in the range of 0.08–0.79 V. The potential of cycled anode was more positive than that of activated anode. Therefore, the lithium-insertion amount of cycled anode was lower than that of activated anode when the full battery finished charging, which was consistent with the XRD result. Because the anode potential after long-term cycles was still above 0 V during the charging process and a high voltage plateau corresponding to the stripping of metal lithium did not appear in the discharge curve after 3200 cycles (Figure 1),[20] metallic lithium did not exist in the deposition layer in combination with the results of XPS and XRD. The depositions on the upper and lower surfaces of MCMB anode were composed of Li_2O,

dx.doi.org/10.1021/am502887v | ACS Appl. Mater. Interfaces 2014, 6, 12962–12970

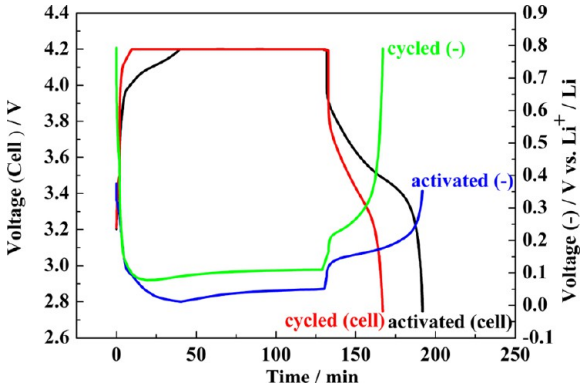

Figure 9. Voltage−time curves of activated and cycled full batteries charged and discharged at 1 C and the corresponding potential of MCMB anodes.

LiF, LiOH, Li_2CO_3, $ROCO_2Li$, and ROLi, so the deposition could be called lithium compound deposition.

3.4. Reasons for the Decline of Lithium-Intercalation Amount in Cycled Anode. Next, the reasons why lithium ions had difficulty entering MCMB and the lithium-insertion amount declined after long-term cycles were examined. Figure 10 shows SEM images of pristine, activated, and long-term cycled MCMB anodes. No obvious changes could be observed in the low-magnification SEM images (Figure 10a−c). In the high-magnification SEM images, AB particles were dispersed on the surface of MCMB particles in the pristine electrode (Figure 10d). Membrane appeared on the surfaces of both activated and cycled MCMB anodes (Figure 10e and f), which tended to smooth the anode surface. According to the literature,[11] the membrane was SEI film. The results indicated that SEI film was formed continuously on the surface of MCMB particles during the long-term cycling.

SEI film on the surface of cycled MCMB anode was removed by water washing. The morphologies of pristine anode (PA, Figure 10d), cycled anode (CA, Figure 10e), and water washed anode (WA, Figure 11) were compared. It could be seen from Figure 11 that no membrane could be observed on WA, and

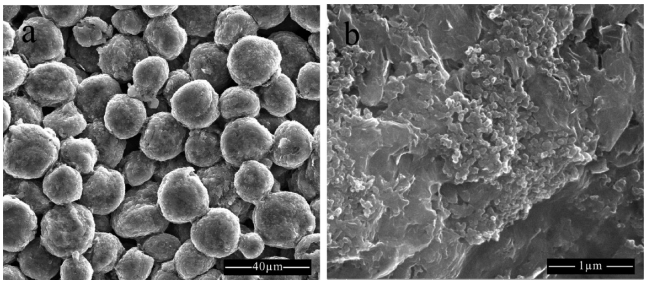

Figure 11. SEM images of cycled anode after water washing. (a) Low-magnification SEM image, (b) high-magnification SEM image.

the morphology has recovered to the state of PA. Therefore, SEI film could be removed basically by water washing.

Figure 12 demonstrated the first lithium-intercalation curves of PA, CA, and WA coin cells at 0.02 C, and the effects of SEI

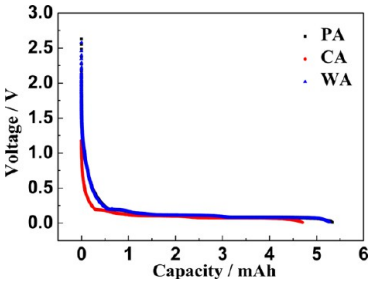

Figure 12. First lithium-intercalation curves of PA, CA, and WA coin cells at 0.02 C.

film on the lithium-intercalation capacity loss of cycled MCMB anode are shown in Table 2. Lithiated capacity of PA was 5.34 mAh, and that of CA was 4.70 mAh. Accordingly, the capacity loss caused by long-term charge/discharge cycles was 0.64 mAh. The capacity of WA recovered to 5.29 mAh after SEI film on cycled anode was removed. By comparing with the capacity of CA, it could be drawn that the capacity loss caused by SEI film was 0.59 mAh. By comparing 5.29 mAh of WA with 5.34

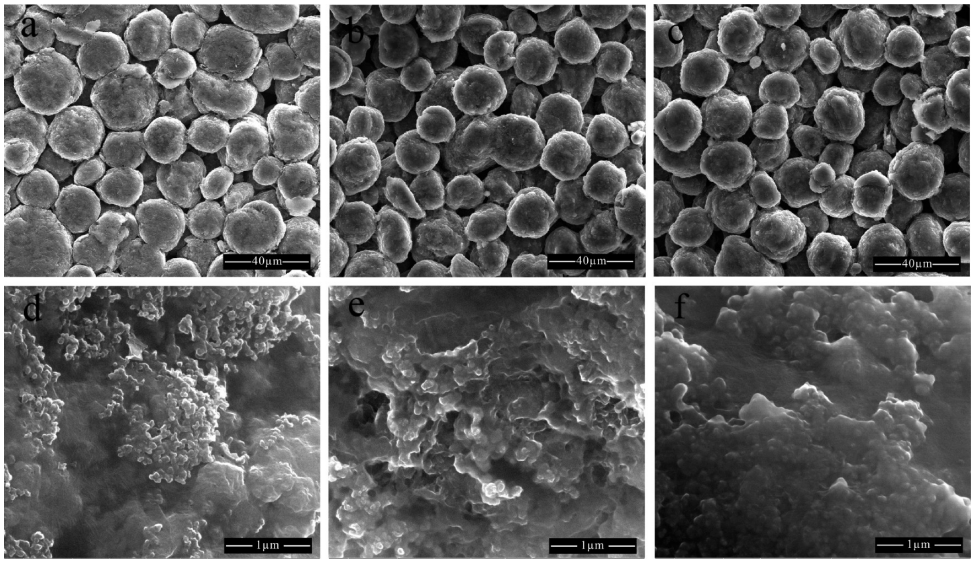

Figure 10. SEM images of pristine, activated, and long-term cycled MCMB anodes. (a,d) Pristine, (b,e) activated, (c,f) long-term cycled.

Table 2. Effects of SEI Film and Other Factors on the Lithium-Intercalation Capacity Loss of Cycled MCMB Anode

	capacity loss (mAh)	capacity loss rate (%, relative to total capacity loss of CA)
CA	0.64	100
SEI film in CA	0.59	92.2
other factors in CA	0.05	7.8

mAh of PA, it could be drawn that the capacity loss caused by other factors except SEI film was 0.05 mAh.

If the total capacity loss of 0.64 mAh was defined as 100%, the capacity loss from SEI film was 92.2%, and that from other factors (such as structure degradation of MCMB,[24] corrosion of current collector,[25,26] and so on) was 7.8%. Accordingly, SEI film generated during long-term cycling reduced lithium-intercalation capacity of anode significantly. The result indicated that SEI film hindered the intercalation of lithium ions into graphite layer significantly.

3.5. Reasons Why Deposition Generated on the Lower Surface of MCMB Anode First and Then on the Upper Surface. MCMB particles, AB, binder, and SEI film existed between the lower and upper surfaces of MCMB layer. These substances could lead to the generation of resistances. Accordingly, the potential of MCMB particles close to the current collector was more negative than that far from the current collector when the full battery was charged. The thickness of SEI film in the anode increased with the decrease of the charging potential.[27] Therefore, SEI film on the lower surface of MCMB layer was thicker, and lithium ions were more difficult to intercalate into graphite layer through SEI film. So lithium ions were more likely to gather on the lower surface of MCMB layer first, and lithium compound deposition was formed. SEI film on the upper surface of MCMB layer was thinner than that on the lower surface, so lithium compound deposition generated on the upper surface of MCMB layer later.

3.6. Effects of $LiCoO_2$ Cathode on the Formation of Deposition. SEI film formed during the long-term cycling could hinder lithium intercalation into the carbon layer, leading to the gather and deposition of lithium ion on the surface of MCMB. However, lithium compound deposition did not appear on the anode surface evenly according to Figures 2 and 3. Consequently, the formation of lithium compound deposition was possibly related to positive electrode besides SEI film on the anode. PC, NC, and LC then were examined by XRD tests.

As could be seen from the curves in Figure 13, the intensities of (003) peak from the three samples were all very large because tested samples were electrodes. Electrodes were pasted, pressed, and so on in the preparation, making the preferred orientation of $LiCoO_2$ happen. Yet it had no effect on the location and shape of peak.[28,29] By comparing the curves in Figure 13b and c, it could be seen that the locations of (003) and (104) in the samples of PC and NC had little difference. However, the two peaks of LC both shifted toward lower angles. Such shifting indicated that lack of lithium occurred in $LiCoO_2$,[29−31] making $LiCoO_2$ in full battery at fully discharged state transform into $Li_{1-x}CoO_2$. The lithium ions lost from $LiCoO_2$ were formed into lithium compound deposition on the surface of MCMB anode.

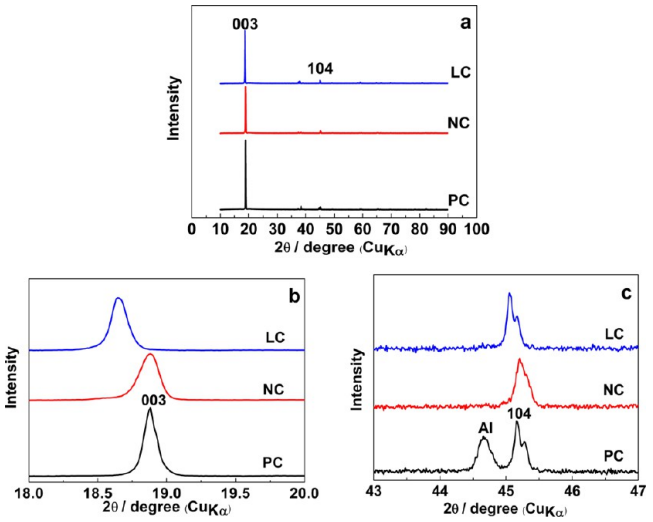

Figure 13. XRD patterns of PC, NC, and LC. Parts (b) and (c) were the enlarged pictures of (a).

Accordingly, there were two reasons why lithium compound deposition could be formed on MCMB anode. On the one hand, SEI film formed during long-term cycling hindered the intercalation of lithium ions into carbon layers. On the other hand, active lithium in cathode provided the source of lithium for the formation of lithium compound deposition. So lithium compound deposition did not generate in some regions of long-term cycled anode, because the corresponding cathode did not provide lithium resource for the formation of lithium compound deposition.

Although the composition of the deposition was similar to that of traditional SEI film, the deposition was different from traditional SEI film because of its dendritic and granular morphology and great thickness. The structural fade of MCMB[24,32] or the gas formation side-reactions[33,34] during the long-term cycles may lead to the fracture of SEI film, and the fresh surface of MCMB was exposed. The electrolyte was reduced on the fresh surface; therefore, the SEI film growth occurred on the surface of MCMB. After a layer of new SEI film was formed on the exposed MCMB surface, SEI film stopped growing unless other exposed MCMB surface appeared. When $LiCoO_2$ cathode provided large amounts of lithium ions for the cycled MCMB anode during the charging and SEI film on the anode hindered these lithium ions from entering carbon layers, the lithium ions gathered on the surface of cycled MCMB anode, and the lithium compound deposition was formed. The appearance of the deposition would hinder lithium ions from entering the carbon layers further, which helped the formation of the deposition further. Accordingly, once the deposition was formed on the surface of MCMB, the growth of deposition would occur during each charging process. Therefore, the thickness of the deposition was much greater than that of SEI film on the surface of MCMB.

4. CONCLUSION

Lithium compound deposition after long-term cycling was investigated using $LiCoO_2$/MCMB battery. The deposition did not generate on the activated anode, but it appeared unevenly on long-term cycled anode. It was formed on the lower surface of MCMB layer first, then on the upper surface. Once the deposition generated on the lower surface of MCMB layer,

MCMB layer and deposition would peel off from the current collector and a bump would be formed in the cycled anode. The exfoliation and thick deposition increased the ohmic resistance, film resistance, and charge transfer resistance of the cell and decreased the capacity significantly. The potential of cycled anode was above 0 V during the lithium-intercalation process, and a high voltage plateau corresponding to the stripping of metal lithium did not appear in the discharge curve of the cycled battery. Moreover, metallic lithium was not detected by XPS and XRD tests; therefore, metallic lithium did not exist in either the upper or the lower deposition layer. The outer regions of depositions on the lower and upper surfaces of MCMB layer both consisted of Li_2CO_3, LiOH, $ROCO_2Li$, and ROLi. The inner region of the etched lower deposition layer mainly consisted of Li_2O, LiF, and Li_2CO_3, and that of the etched upper deposition layer mainly consisted of Li_2CO_3, $ROCO_2Li$, ROLi, and LiF. There were two reasons for the formation of lithium compound deposition during long-term cycling. On the one hand, SEI film formed during long-term cycling hindered the intercalation of lithium ions into carbon layers. On the other hand, active lithium in cathode provided the source of lithium for the formation of lithium compound deposition. Because SEI film on the lower surface of MCMB layer was thicker than that on the upper surface, lithium compound deposition generated on the lower surface first.

AUTHOR INFORMATION

Corresponding Authors

*Tel.: +86-451-86413721. E-mail: chengxq@hit.edu.cn.
*Tel.: +86-451-86413707. E-mail: yingeping@hit.edu.cn.

Notes

The authors declare no competing financial interest.

ACKNOWLEDGMENTS

We would like to thank the National High Technology Research and Development Program (863 Program) of China (no. 2012AA110203) for financial support.

REFERENCES

(1) Christensen, J.; Albertus, P.; Sanchez-Carrera, R. S.; Lohmann, T.; Kozinsky, B.; Liedtke, R.; Ahmed, J.; Kojic, A. A Critical Review of Li/Air Batteries. *J. Electrochem. Soc.* **2012**, *159*, R1−R30.

(2) Lee, J.-S.; Kim, S. T.; Cao, R.; Choi, N.-S.; Liu, M.; Lee, K. T.; Cho, J. Metal-Air Batteries with High Energy Density: Li-Air versus Zn-Air. *Adv. Energy Mater.* **2011**, *1*, 34−50.

(3) Bruce, P. G.; Freunberger, S. A.; Hardwick, L. J.; Tarascon, J.-M. Li-O_2 and Li-S Batteries with High Energy Storage. *Nat. Mater.* **2012**, *11*, 19−29.

(4) Aurbach, D.; Pollak, E.; Elazari, R.; Salitra, G.; Kelley, C. S.; Affinito, J. On the Surface Chemical Aspects of Very High Energy Density, Rechargeable Li-Sulfur Batteries. *J. Electrochem. Soc.* **2009**, *156*, A694−A702.

(5) Aurbach, D.; Gofer, Y. The Correlation between Surface Chemistry, Surface Morphology, and Cycling Efficiency of Lithium Electrodes in a Few Polar Aprotic Systems. *J. Electrochem. Soc.* **1989**, *136*, 3198−3205.

(6) Yoshimatsu, I.; Hirai, T.; Yamaki, J.-I. Lithium Electrode Morphology during Cycling in Lithium Cells. *J. Electrochem. Soc.* **1988**, *135*, 2422−2427.

(7) Shiraishi, S.; Kanamura, K.; Takehara, Z.-I. Surface Condition Changes in Lithium Metal Deposited in Nonaqueous Electrolyte Containing HF by Dissolution-Deposition Cycles. *J. Electrochem. Soc.* **1999**, *146*, 1633−1639.

(8) Kanamura, K.; Shiraishi, S.; Takehara, Z.-I. Electrochemical Deposition of Uniform Lithium on an Ni Substrate in a Nonaqueous Electrolyte. *J. Electrochem. Soc.* **1994**, *141*, L108−L110.

(9) López, C. M.; Vaughey, J. T.; Dees, D. W. Insights into the Role of Interphasial Morphology on the Electrochemical Performance of Lithium Electrodes. *J. Electrochem. Soc.* **2012**, *159*, A873−A886.

(10) López, C. M.; Vaughey, J. T.; Dees, D. W. Morphological Transitions on Lithium Metal Anodes. *J. Electrochem. Soc.* **2009**, *156*, A726−A729.

(11) Yang, L.; Cheng, X.; Ma, Y.; Lou, S.; Cui, Y.; Guan, T.; Yin, G. Changing of SEI Film and Electrochemical Properties about MCMB Electrodes during Long-Term Charge/Discharge Cycles. *J. Electrochem. Soc.* **2013**, *160*, A2093−A2099.

(12) Wu, M.-S.; Chiang, P.-C. J.; Lin, J.-C. Electrochemical Investigations on Advanced Lithium-Ion Batteries by Three-Electrode Measurements. *J. Electrochem. Soc.* **2005**, *152*, A47−A52.

(13) Spotnitz, R.; Franklin, J. Abuse Behavior of High-Power, Lithium-Ion Cells. *J. Power Sources* **2003**, *113*, 81−100.

(14) Tobishima, S.-I.; Yamaki, J.-I. A Consideration of Lithium Cell Safety. *J. Power Sources* **1999**, *81−82*, 882−886.

(15) Park, G.; Gunawardhana, N.; Nakamura, H.; Lee, Y.-S.; Yoshio, M. The Study of Electrochemical Properties and Lithium Deposition of Graphite at Low Temperature. *J. Power Sources* **2012**, *199*, 293−299.

(16) Lu, W.; López, C. M.; Liu, N.; Vaughey, J. T.; Jansen, A.; Dees, D. W. Overcharge Effect on Morphology and Structure of Carbon Electrodes for Lithium-Ion Batteries. *J. Electrochem. Soc.* **2012**, *159*, A566−A570.

(17) Tippmann, S.; Walper, D.; Balboa, L.; Spier, B.; Bessler, W. G. Low-Temperature Charging of Lithium-Ion Cells Part I: Electrochemical Modeling and Experimental Investigation of Degradation Behavior. *J. Power Sources* **2014**, *252*, 305−316.

(18) Huang, C.; Zhuang, S.; Tu, F. Electrode/Electrolyte Interfacial Behaviors of $LiCoO_2$/Mixed Graphite Li-Ion Cells during Operation and Storage. *J. Electrochem. Soc.* **2013**, *160*, A376−A382.

(19) Zhang, S. S.; Xu, K.; Jow, T. R. Study of the Charging Process of a $LiCoO_2$-Based Li-Ion Battery. *J. Power Sources* **2006**, *160*, 1349−1354.

(20) Smart, M. C.; Ratnakumar, B. V. Effects of Electrolyte Composition on Lithium Plating in Lithium-Ion Cells. *J. Electrochem. Soc.* **2011**, *158*, A379−A389.

(21) Lin, H.-p.; Chua, D.; Salomon, M.; Shiao, H.-C.; Hendrickson, M.; Plichta, E.; Slane, S. Low-Temperature Behavior of Li-Ion Cells. *Electrochem. Solid-State Lett.* **2001**, *4*, A71−A73.

(22) Oumellal, Y.; Delpuech, N.; Mazouzi, D.; Dupré, N.; Gaubicher, J.; Moreau, P.; Soudan, P.; Lestriez, B.; Guyomard, D. The Failure Mechanism of Nano-Sized Si-Based Negative Electrodes for Lithium Ion Batteries. *J. Mater. Chem.* **2011**, *21*, 6201−6208.

(23) Moss, P. L.; Au, G.; Plichta, E. J.; Zheng, J. P. Study of Capacity Fade of Lithium-Ion Polymer Rechargeable Batteries with Continuous Cycling. *J. Electrochem. Soc.* **2010**, *157*, A1−A7.

(24) Hardwick, L. J.; Marcinek, M.; Beer, L.; Kerr, J. B.; Kostecki, R. An Investigation of the Effect of Graphite Degradation on Irreversible Capacity in Lithium-Ion Cells. *J. Electrochem. Soc.* **2008**, *155*, A442−A447.

(25) Braithwaite, J. W.; Gonzales, A.; Nagasubramanian, G.; Lucero, S. J.; Peebles, D. E.; Ohlhausen, J. A.; Cieslak, W. R. Corrosion of Lithium-Ion Battery Current Collectors. *J. Electrochem. Soc.* **1999**, *146*, 448−456.

(26) Kawakita, J.; Kobayashi, K. Anodic Polarization Behavior of Copper in Propylene Carbonate. *J. Power Sources* **2001**, *101*, 47−52.

(27) Zhong, K.; Xia, X.; Zhang, B.; Li, H.; Wang, Z.; Chen, L. MnO Powder as Anode Active Materials for Lithium Ion Batteries. *J. Power Sources* **2010**, *195*, 3300−3308.

(28) Ohzuku, T.; Ueda, A. Solid-State Redox Reactions of $LiCoO_2$ (R3m) for 4 V Secondary Lithium Cells. *J. Electrochem. Soc.* **1994**, *141*, 2972−2977.

(29) Ueda, A.; Ohzuku, T. Solid-State Redox Reactions of $LiNi_{1/2}Co_{1/2}O_2$ (R3m) for 4 V Secondary Lithium Cells. *J. Electrochem. Soc.* **1994**, *141*, 2010−2014.

(30) Maher, K.; Yazami, R. Effect of Overcharge on Entropy and Enthalpy of Lithium-Ion Batteries. *Electrochim. Acta* **2013**, *101*, 71−78.
(31) Maher, K.; Yazami, R. A Study of Lithium Ion Batteries Cycle Aging by Thermodynamics Techniques. *J. Power Sources* **2014**, *247*, 527−533.
(32) Liu, P.; Wang, J.; Hicks-Garner, J.; Sherman, E.; Soukiazian, S.; Verbrugge, M.; Tataria, H.; Musser, J.; Finamore, P. Aging Mechanisms of $LiFePO_4$ Batteries Deduced by Electrochemical and Structural Analyses. *J. Electrochem. Soc.* **2010**, *157*, A499−A507.
(33) Lanz, M.; Novák, P. DEMS Study of Gas Evolution at Thick Graphite Electrodes for Lithium-Ion Batteries: the Effect of γ-Butyrolactone. *J. Power Sources* **2001**, *102*, 277−282.
(34) Imhof, R.; Novák, P. In Situ Investigation of the Electrochemical Reduction of Carbonate Electrolyte Solutions at Graphite Electrodes. *J. Electrochem. Soc.* **1998**, *145*, 1081−1087.